Thin $Si_xN_yC_z$ films deposited from hexamethyldisilazane by RF PECVD technique for optical filter applications

Katarzyna Oleśko[1], Hieronim Szymanowski[1], Maciej Gazicki-Lipman[1],
Jacek Balcerzak[2], Witold Szymański[1], Wojciech Pawlak[1],
Anna Sobczyk-Guzenda[1,*]

[1]Institute of Materials Science and Engineering, Lodz University of Technology, Stefanowskiego 1/15, 90-924 Lodz, Poland

[2]Department of Molecular Engineering, Faculty of Process and Environmental Engineering, Lodz University of Technology, Wolczanska 213, 90-924 Lodz, Poland

This work initiates a series of reports aimed at a construction of rugate optical filters based on silicon rich materials of alternating gradients of refractive index n with the help of plasma enhanced chemical vapor deposition (PECVD) technique, The idea is to start deposition of high refractive index Si_xN_y type of material using hexamethyldisilazane (HMDSN) vapor and nitrogen rich atmosphere, and then to gradually replace nitrogen with oxygen in that atmosphere in order to lower n down to a minimum characteristic of Si_xO_y type of material. A return to initial gas composition should increase the index back to its maximum. In the present work, thin $Si_xN_yC_z$ films were synthesized from a mixture of HMDSN vapor with gaseous NH_3 and N_2. The effect of NH_3/N_2 ratio on the coating morphology, its elemental composition, chemical bonding and optical properties was studied using scanning electron microscopy, X-ray photoelectron spectroscopy, Fourier transform infrared spectroscopy, ultra-violet absorption spectroscopy and variable angle spectroscopic ellipsometry. The results show that films of the highest index of refraction and the lowest extinction coefficient have been deposited from the gas mixture containing 90 % of ammonia. These coatings are also characterized by the lowest carbon and the highest nitrogen contents.

Keywords: *HMDSN; PECVD; refractive index; chemical structure; adhesion*

1. Introduction

Today, stack multilayer optical interference filters are used in numerous fields of application including astronomy, commercial lens, optical fiber production and telecommunication. They may be manufactured with a number of such thin film technologies as magnetron sputtering [1, 2], sol-gel method [3–5], and plasma enhanced chemical vapor deposition (PECVD) [6–8]. There is, however, one major setback often hindering the work of these devices. Since a principal requirement concerning subsequent layers of a filter regards as large as possible difference in the magnitude of their indices of refraction, it is frequently fulfilled at the expense of adherence between these layers, therefore, endangering the device longevity. A solution of this problem has come with

the so called "rugate" interference filters, wherein a stack of discretely interchanging layers of high and low refractive index is replaced with a single layer characterized by a continuously alternating magnitude of that index [9]. Not only is the adhesion problem inexistent in such constructions, but very often their optical characteristics are substantially improved compared to the stack type devices. The improvement basically consists in an elimination of secondary harmonic bands from the transmission spectra of interference filters.

Due to their valuable properties, such as substantial hardness [10], good chemical resistance [11], high resistance against oxidation [12], low friction coefficient [13] and broad energy gap [14], both silicon nitrides (Si_xN_y) and silicon carbonitrides ($Si_xN_yC_z$) constitute a subject of a substantial technological interest. As thin solid films, these materials are applied in UV radiation detectors [15], photoluminescence diodes,

*E-mail: anna.sobczyk-guzenda@p.lodz.pl

solar cells [16], humidity sensors [17], thermal diffusion barriers [18], as well as in a number of biomedical appliances [2, 19]. In the latter applications, they are also used in a form of nanoparticles [20]. Thanks to advantageous optical properties, especially to their high index o refraction and low extinction coefficient, thin Si_xN_y and $Si_xN_yC_z$ films may also be used in a construction of optical filters. The most common techniques of their deposition comprise magnetron sputtering (MS) [10, 13, 21–23], hot wire chemical vapor deposition (HWCVD) [16] and plasma enhanced chemical vapor deposition (PECVD) [17].

The present report initiates a series of investigations purposefully directed to a construction of rugate optical filters based on gradient silicon nitride/silicon oxide type of materials of sinusoidally alternating magnitude of refractive index. In this work, radiofrequency (RF) PECVD technique has been applied for the purpose of synthesizing optical grade thin $Si_xN_yC_z$ films. In the PECVD method of deposition of silicon containing films, either gaseous silane (SiH_4) [24, 25] or liquid organosilicones [26–29] are used as precursors. The latter group of compounds has two significant advantages over SiH_4– on the one hand they offer a substantial safety improvement compared to extremely flammable silane and, on the other, they are often more economical. In addition, when a presence of such heteroatoms as nitrogen or oxygen is required in the coating, either organosilazanes or organosiloxanes may be used as precursors for the two elements. An incorporation of the third main element present in organosilicone connections, namely carbon, constitutes an obvious disadvantage of such a solution, however, the shortcomings are not too detrimental in the case of optical applications.

In the present work, a combination of hexamethyldisilazane (HMDSN) vapor with a gaseous mixture of ammonia and nitrogen is used as a source material. Both structure of the resulting coatings and their optical properties are studied as a function of ammonia concentration in the starting atmosphere. Thickness and optical constants of the films are determined by means of variable angle spectroscopic ellipsometry (VASE), while their elemental composition and chemical bonding are examined with the help of X-ray photoelectron spectroscopy (XPS) and Fourier transform infrared (FT-IR) spectroscopy, respectively. Finally, such mechanical properties of the coatings as their adhesion, hardness and modulus of elasticity are studied with the nanointendation method.

2. Experimental

2.1. Materials

The following chemicals were used as source materials for particular elements: Sigma Aldrich hexamethyldisilazane (HMDSN) of a 99 % purity as a source of silicon and a mixture of gaseous nitrogen of a 99.999 % purity with gaseous ammonia of a 99.98 % purity (contaminated with: $H_2O \leqslant$ 5 ppm, $O_2 \leqslant$ 5 ppm, $N_2 \leqslant$ 30 ppm, $CO \leqslant$ 5 ppm, $CO_2 \leqslant$ 1 ppm, KW/HC $\leqslant$ 2 ppm, both supplied by Linde Gas Polska sp. z o.o., as a source of nitrogen.

As substrates, either p-type 500 μm thick pieces of silicon wafers of $\langle 1\ 1\ 1 \rangle$ orientation or 25 × 25 mm boron-silica glass slides, or slices of 1H18N9 steel of a diameter of 16 mm, were applied.
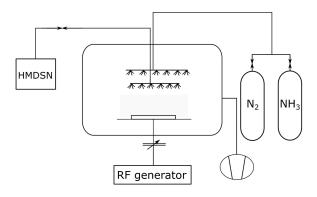

Fig. 1. Schematic representation of the RF PECVD deposition system.

2.2. Deposition procedure

Schematic representation of the RF PECVD reactor used in this work is shown in Fig. 1.

In this reactor, substrates are placed directly on the lower, hot electrode powered from an Advance Energy, model Cesar radiofrequency generator operating at 13.56 MHz and coupled with a matching network. In order to stabilize its temperature and to enable deposition on thermolabile substrates, this electrode is cooled with circulating water. The grounded counter electrode is comprised of the main reactor body. Working gases, namely a gaseous mixture of N_2 with NH_3 as well as HMDSN vapors are introduced to the upper section of the reactor chamber with the flow rate being controlled by means of MKS MFC, model MF1 flow controllers. Their uniform distribution inside the reactor is assured by two separate shower type internal supply lines. The vacuum support system consists of a main vacuum line, two Swagelok valves (one pressure control valve and one on-off valve) of an Oerlikon Leybold mechanical vacuum pump. System pressure is monitored with the help of Thermovac, model TTR 91 pressure gauge.

Table 1. Main parameters of deposition process.

Initial pressure	2.5 Pa
Power of deposition	300 W
Deposition time	90 s; 480 s
Flow rate of HMDSN	5.8 sccm
Flow rate of NH_3	0-200 sccm
Flow rate of N_2	200-0 sccm

The magnitudes of the main parameters of the deposition process are shown in Table 1. Prior to each run, the chamber was evacuated down to 2.5 Pa. In all the processes, the flow rate of HMDSN was maintained at the same level of 5.8 sccm, with the principal operational parameter being the NH_3/N_2 ratio in the precursor mixture, varied between 0 % and 100 %. The flow rates values of both gaseous components were varied from 0 to 200 sccm, with the magnitude of the joint flow rate always remaining at 200 sccm. Constant deposition power of 300 W was used in all the processes. In order to obtain similar thickness ($\sim$500 nm), different deposition times were applied: 90 s for stainless steel and 480 s for the remaining substrates.

2.3. Film diagnostics

2.3.1. Optical properties

Optical properties of the films as well as their thickness were determined with the help of J.A. Woollam Co. variable angle spectroscopic ellipsometer (VASE), working at three different angles of incidence, namely 65°, 70° and 75°. The measurements were carried out within a spectral range of 350 nm to 1000 nm, with a single step of 2 nm, using film specimen deposited on silicon substrates. The data obtained were processed with the help of WVASE software with an application of the Cauchy model. The mean square error of the model fitting amounted to MSE = 17.

Optical transmission of the films within the spectral range of 200 nm to 900 nm was determined with the help of a ThermoScientific ™Evolution 220 UV-Vis systems for samples deposited on glass substrates.

2.3.2. Morphology

In order to evaluate a large area surface morphology of the coatings, a Carl Zeiss ULTRAPlus scanning electron microscope (SEM), supported with the SmartSEM software, was used. The microscope was equipped with a FEG type cathode, which allowed one to conduct observation at low accelerating voltage in the range of 0.5 kV to 30 kV. In order to dissipate the surface charge collected at the specimen surface, a Carl Zeiss Charge Compensator mechanism was used. This mechanism enabled an observation of samples of poor electrical conductivity as well as that of non-conductive samples. For the purpose of scanning the $Si_xN_yC_z$ specimens, an accelerating voltage of 2.5 kV and a distance of approximately 6 mm were applied. Under such experimental conditions it was critical that the samples were not modified in any way. For creating images, a magnification of 10 000× was used.

2.3.3. Chemical composition

The FT-IR analysis was performed within the spectral range of 4000 cm^{-1} to 500 cm^{-1}, with the resolution of 4 cm^{-1}, using ThermoScientific FT-IR spectrometer model Nicolet iS50. DTGS KBr beam splitter was applied in the work,

which was carried out in an absorbance mode. A single measurement cycle was comprised of 64 scans. The resulting spectra were thickness normalized.

The XPS measurements were carried out with a Kratos AXIS Ultra spectrometer using monochromatic AlKα X-rays source of an excitation energy of 1486.6 eV. The spectra were obtained using an analysis area of 300 μm × 700 μm. The power of anode was set at 150 W and the hemispherical electron energy analyzer was operated at a pass energy of 20 eV for all the high resolution measurements. All measurements were performed with the use of a charge neutralizer and every spectrum was scanned ten times in order to increase the signal-to-noise-ratio. Evaluation of XPS data was conducted using a Kratos Vision 2 software. Each specimen was XPS sampled at three different positions with the mean value and the measurement error being determined from the three results obtained. The background subtraction was performed with Shirley algorithm and the adventitious carbon main peak (C 1s, 284.8 eV) was used for a final calibration of each spectrum.

2.3.4. Mechanical properties

Mechanical properties, namely hardness H and modulus of elasticity E of the coatings were measured using nanoindentation technique with the help of G200 nanoindenter system. In order to determine H and E, nine intendations with a Berkovich type diamond intender of a face angle equal 65.3° and a tip roundness r < 20 nm were performed on each sample. A continuous stiffness measurement (CSM) method was used for that purpose. The method consists in a continuous measurement of contact stiffness S in a course of material penetration and it allows one to perform recording of its mechanical properties as a function of penetration depth h. In this way, one is easily able to eliminate those H and E values which are affected by interaction with the substrate. Taking into account the value of Berkovich tip roundness and theoretical 10 % of coating thickness rule, one can state that a threshold coating thickness, above which the substrate does not

affect the measurement, amounts to approximately 200 nm. This is well below the values obtained in this work, where an approximate thickness of a coating equals 500 nm. Each intendation was performed with a constant strain rate of 0.05 s^{-1} and the data collected were analyzed using Oliver and Pharr procedure [30].

For adhesion measurements, a standard scratch test with lateral force measurement was applied. The measurement of forces lateral with respect to X-Y plane allows one to compute friction coefficient μ. A critical delamination force Fc is then determined by an analysis of changes of that friction coefficient, as well as of penetration curves, with the help of optical microscope observations. In order to determine Fc, five scratches with diamond conical tip of apex angle equal 90° and a roundness of 1 μm were made on each sample. With a load increasing from 0 mN to 20 mN at a constant rate of 0.2 mN/μm, an approximate length of a scratch should equal 100 μm.

3. Results and discussion

Film diagnostics was performed for two different purposes, one utilitarian and one cognitive. First of all, testing optical properties of the coatings with the VASE technique was aimed at maximizing the magnitude of their refractive index n. The respective values for the commercial amorphous films of pure silicon nitride (Si_3N_4) amount to 1.93 to 2.08 [31]. Coatings which additionally contain carbon should be characterized by slightly lower indices. For the sake of filter construction, however, an important feature is the highest possible difference between high and low refractive index material. Since the low n component is designed to be a film of amorphous silicon dioxide having the n value of 1.45 [32], maximizing that index in the case of $Si_xN_yC_z$ films synthesized in this work was our ultimate goal. Utilitarian reasons were also directly connected to the SEM morphology studies of the films and their mechanical testing. An excessive surface roughness may lead to light scattering which rules out optical applications of a material while such mechanical

properties as adhesion, hardness and elasticity modulus are crucial for any thin film application.

The second purpose of film diagnostics was of a much more cognitive character. XPS studies allow one to determine elemental composition of the films and their bonding which, when correlated with the results of FT-IR measurements, also recording a presence of different chemical bonds in the material structure, may lead to better understanding of this material chemical constitution.
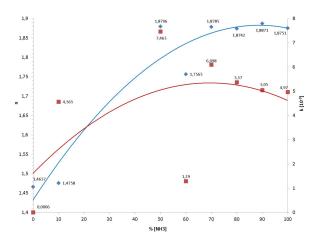

Fig. 2. Values of refractive index n and extinction coefficient k, (determined at 550 nm) for samples deposited at different ammonia content in the NH$_3$/N$_2$ mixture.

3.1. Optical properties

Ellipsometric measurements with an application of Cauchy model were used to determine thickness of the films as well as their optical properties such as index of refraction and extinction coefficient in a broad spectral range. For the sake of comparison, in the following discussion both parameters are presented for the specified wavelength of 550 nm. An analysis of the results allows one to characterize changes of the coating properties resulting from different magnitudes of ammonia to nitrogen ratio in the precursor mixture. In each case, the mean thickness of the samples remains in the range of 505 nm to 540 nm. A dependence of refractive index n and extinction coefficient k on the content of ammonia in the starting NH$_3$/N$_2$ mixture is presented in Fig. 2.

As seen in the figure, an increase in ammonia content in the precursor mixture results in a substantial increase of the film refractive index from an approximate value of 1.46 to an approximate value of 1.88, with an evident tendency to saturate for films deposited at NH$_3$ content exceeding 50 %. As far as their extinction coefficient is concerned, its magnitude remains at relatively low level, on average amounting to 5.05×10^{-3}, nearly independent of the content of ammonia in the starting material. Since extinction coefficient of a material is a parameter revealing absorption of light in that material, its low magnitude (such as the ones obtained in this study) constitutes a property very advantageous from a point of view of a construction of optical filters.

Dispersion curves of n and k optical parameters for the coating deposited at 90 % of ammonia content in the reaction mixture are presented in Fig. 3. Their course is characteristic of optical coatings of high quality.
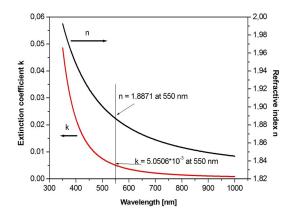

Fig. 3. Optical dispersion curves of the coating deposited at 90 % of ammonia.

Transmission spectra, recorded in the spectral range of 200 nm to 900 nm, of a plain glass substrate as well as of those coated with Si$_x$N$_y$C$_z$ films deposited at 50 % and at 90 % of ammonia content in the NH$_3$/N$_2$ mixture, are presented in Fig. 4. In this figure, high transmission magnitudes result from low extinction and, therefore, they confirm the data obtained with the ellipsometric

measurements. In general, all the results presented consequently show that the larger ammonia content in the precursor mixture, the higher is the refractive index of the film synthesized from that mixture and the lower is its absorption threshold. In other words, films deposited at maximum content of ammonia are characterized by the best optical quality.
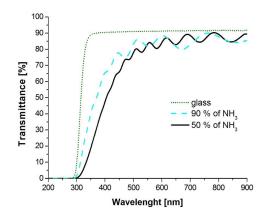

Fig. 4. Transmission spectra of an uncoated glass substrate and of substrates coated with films deposited at 50 % and at 90 % of ammonia.

3.2. Structure and chemical composition

3.2.1. Scanning Electron Microscopy

Plan-view scanning electron micrographs of the films deposited at 50, 70 and 90 % of NH$_3$ content are presented in Fig. 5A, Fig. 5B and Fig. 5C, respectively. As seen in the figures, all the coatings have a solid compact structure and they are free of cracks. As far as their homogeneity is concerned, the coating deposited at 50 % of ammonia (Fig. 5A) appears to be the least homogenous one, exhibiting surface globular features of dimensions in the 0.1 μm to 0.4 μm range. With an increasing content of ammonia in the working atmosphere, both the average dimension and the number of the globules decrease. When one disregards a presence of dust contamination (either due to powder formation or gained in the handling phase of the samples) the sample shown, shown in Fig. 5C, may be considered as very smooth and reproducing morphology of the silicon substrate. This result is

confirmed by roughness data obtained from ellipsometric measurements which, on average, amounts approximately 5 nm.

Fig. 5. Surface SEM micrographs of the films deposited at: 50 % of ammonia (A), 70 % of ammonia (B) and 90 % of ammonia (C) in the NH$_3$/N$_2$ mixture. Magnification 10 000×.

3.2.2. Fourier Transform Infrared Spectroscopy

FT-IR spectra of the coatings deposited at three different magnitudes of NH$_3$ content in the starting atmosphere, namely those of 50 %, 70 % and 90 %, are presented in Fig. 6.
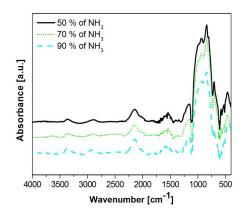

Fig. 6. FT-IR spectra of the films deposited at different ammonia content in the reaction mixture.

In each of the three spectra shown in Fig. 6, there is a number of infrared absorption bands characteristic of certain types of vibrations of different chemical bonds usually present in Si$_x$N$_y$C$_z$ films. For the sake of clarity and comparison, these bands are organized in the following absorption ranges:

- the 3450 cm^{-1} to 3220 cm^{-1} range, with characteristic stretching vibrations of

O–H (3370 cm^{-1}) and N–H (3350 and 3320 cm^{-1}) bonds,

- the 3000 cm^{-1} to 2800 cm^{-1} range, with characteristic stretching vibrations of C–H$_x$ bonds,

- the 2300 cm^{-1} to 1950 cm^{-1} range, with characteristic stretching vibrations of Si–H (2150 cm^{-1}) and Si–N$_3$ (2050 cm^{-1}) bonds,

- the 1730 cm^{-1} to 1440 cm^{-1} range, with characteristic stretching vibrations of C=O (1720 cm^{-1}), C=C (1650 cm^{-1}) and N–O (1550 cm^{-1}) bonds as well as scissoring vibrations of N–H (1630 cm^{-1}) and bending vibrations C–H (1480 cm^{-1} to 1450 cm^{-1}) bonds,

- the 1280 cm^{-1} to 1110 cm^{-1} range, with characteristic stretching vibrations of Si–CH$_3$ and Si–CH$_2^-$ (1270 cm^{-1} to 1250 cm^{-1}) bonds, stretching vibrations of C–O–C (1233 cm^{-1} to 1200 cm^{-1}) bonds, asymmetric stretching vibrations of Si–NH (1180 cm^{-1}) and asymmetric stretching vibrations of Si–O (1160 cm^{-1}) bonds,

- the 1110 cm^{-1} to 610 cm^{-1} range, with characteristic asymmetric stretching vibrations of Si–O (1010 cm^{-1}) bonds, Si–NH–Si (940 cm^{-1}) bonds; and Si–N (845 cm^{-1}) bonds, vibrations of Si–C (805 cm^{-1}) bonds and bending vibrations of C=C (710 cm^{-1}) bonds [33, 34].

In only one of the above IR absorption regions, namely that of 1740 cm^{-1} to 1440 cm^{-1}, no recordable changes of absorption band intensity were detected for films deposited at different experimental conditions. Therefore, this region was neglected in the further discussion of the FT-IR spectra of the Si$_x$N$_y$C$_z$ films under consideration. All the remaining ranges of absorption are presented in Fig. 7, Fig. 8, Fig. 9, Fig. 10 and Fig. 11. In each absorption range, specified in the corresponding figure caption, there are altogether six spectra of the films deposited at 50 %, 60 %, 70 %, 80 %, 90 % and 100 % of ammonia content in the starting NH$_3$/N$_2$ mixture presented.
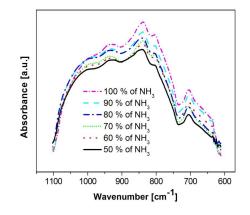

Fig. 7. IR absorption range of 1100 cm^{-1} to 600 cm^{-1} of the films deposited at different ammonia content in the reaction mixture.
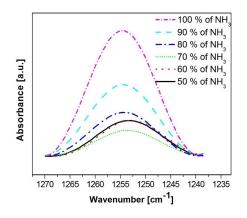

Fig. 8. IR absorption range of 1270 cm^{-1} to 1235 cm^{-1} of the films deposited at different ammonia content in the reaction mixture.

The absorption range of 1110 cm^{-1} to 610 cm^{-1} is presented in Fig. 7. It is a range where the smallest differences in band intensity between films deposited at diverse conditions are observed, with the absorption maxima corresponding to the vibrations of such chemical bonds as Si–O, Si–N and Si–C [49]. The range between 1280 cm^{-1} and 1110 cm^{-1} can be divided into two parts: one covering the 1230 cm^{-1} to 1110 cm^{-1} spectral region where no substantial changes of intensity are detected and the other between 1270 cm^{-1} and 1240 cm^{-1}, presented in Fig. 8, where maxima corresponding to the vibrations of Si–CH$_3$ and Si–CH$_2$– groups are

recorded. They form a broad absorption band, whose intensity increases substantially with an increase of NH_3 content in the precursor atmosphere. Such connections very likely originate from those molecular parts of hexamethyldisilazane that remain unfragmented in the course of the glow discharge. Similar relationship is revealed by the absorption in the 3000 cm^{-1} to 2800 cm^{-1} range shown in Fig. 9. A presence of CH_x connections is confirmed in all the films, whose absorption spectra are displayed in that figure, with the most evident maxima recorded in the case of the coatings deposited at high ammonia content in the precursor atmosphere. The wavenumber range discussed is characteristic of stretching vibrations of carbon-hydrogen bonds in various alkyl environments. Absorption maxima recorded at the wavenumbers of 2890 cm^{-1} and 2948 cm^{-1} originate, respectively, from symmetric and asymmetric stretching vibrations of C–H bonds in methyl (–CH_3) groups [35], while the maxima corresponding to similar vibrations of these bonds in methylene (–CH_2–) groups are recorded at 2860 cm^{-1} and at 2915 cm^{-1}.

range, indicating that an increase of ammonia concentration in the starting atmosphere results in a substantial rise of silicon bound hydrogen content in the resulting films. Apart from those corresponding to Si–H bond vibrations, there is still another maximum present in the spectral range discussed.

Fig. 10. IR absorption range of 2300 cm^{-1} to 2000 cm^{-1} (Si–H bond stretching vibration region) of the films deposited at different ammonia content in the reaction mixture.
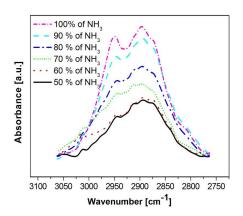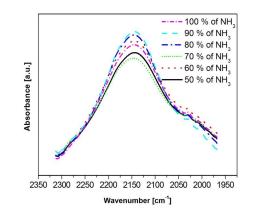

Fig. 9. IR absorption range of 3100 cm^{-1} to 2750 cm^{-1} (C–H bond stretching vibration region) of the films deposited at different ammonia content in the reaction mixture.
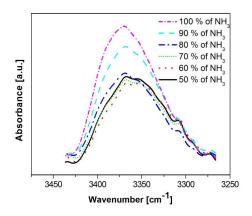

Fig. 11. IR absorption range of 3450 cm^{-1} to 3250 cm^{-1} of the films deposited at different ammonia content in the reaction mixture.

Fig. 10 presents the spectral range of infrared absorption generally corresponding to stretching vibrations of silicon-hydrogen bonds [34, 35]. A tendency should also be noted in this absorption

A presence of N–H bond in the films has been demonstrated by the absorption shown in Fig. 11. It relates to the absorption maxima at 3320 cm^{-1} and at 3350 cm^{-1}, assigned to stretching vibrations of NH groups and to stretching vibrations of NH_2

groups [35], respectively. As seen in the figure, an increase of NH_3 content in the starting mixture results in a substantial rise of both maxima, and of the latter one in particular. The largest band in this range, namely that peaking at the wavenumber of 3370 cm^{-1}, is a band originating from stretching vibrations of –OH groups. The intensity of this band also increases with an increasing concentration of ammonia in the starting atmosphere.

3.2.3. X-ray photoelectron spectroscopy

An XPS analysis was performed in order to determine both atomic composition and chemical bonding of the $Si_xN_yC_z$ films under investigation. An example of full range XPS spectrum of such a coating is presented in Fig. 12.
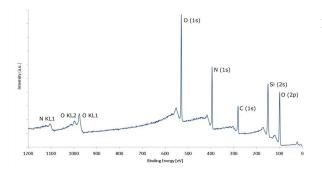

Fig. 12. An example of a survey XPS spectrum of RF PECVD synthesized $Si_xN_yC_z$ film.

A presence of the O(1s) line in the XPS spectra of the films is likely due to two different reasons. One results from their post-deposition contact with atmospheric oxygen, while the other may be connected with water contamination of gaseous ammonia used in the study.

Particular Si(2p), N(1s) and C(1s) core level spectra, extended and deconvoluted, of the samples deposited at 50 % and at 90 % of ammonia in the starting mixture are presented in Fig. 13, Fig. 14 and Fig. 15, respectively. Deconvolution of each core level spectra has been carried out with an assumption of a Gauss distribution. As seen in Fig. 13, the Si(2p) band has been split into three lines, corresponding to silicon atoms bound to carbon, nitrogen and oxygen. In the case of the sample deposited at 50 % of ammonia in the mixture, these

lines are characterized by binding energy values of 101.46 eV, 102.16 eV and 103.76 eV, respectively, while the same lines for the sample synthesized at 90 % of ammonia peak at 101.52 eV, 102.22 eV and 103.72 eV [36–39]. In addition, a detailed analysis of chemical shift values shows that the shift assigned above to Si–N bonding falls to a very close vicinity of a theoretical line corresponding to pure Si_3N_4 [40].
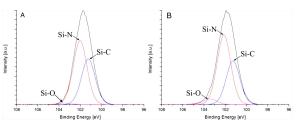

Fig. 13. Deconvolution of Si(2p) XPS core level spectrum for films made at 50 % (A) and 90 % (B) of NH_3.
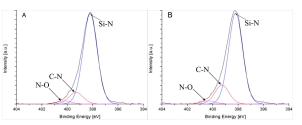

Fig. 14. Deconvolution of N(1s) XPS core level spectrum for films made at 50 % (A) and 90 % (B) of NH_3.

In the nitrogen N(1s) band, presented in Fig. 14, the following contributions have been selected in the spectrum of the 50 % sample: 398.26 eV (Si–N), 399.55 eV (C–N) and 400.36 eV (N–O), while in the 90 % sample the same lines appear at: 398.22 eV (Si–N), 399.42 eV (C–N) and 400.32 eV (N–O) [24]. Finally, the C(1s) band, shown in Fig. 15, can be deconvoluted into four separate contributions corresponding to C–Si, C–C, C–N and C=O bonds. These contributions are the same for 284.05 eV, 285.05 eV, 285.96 eV and 287.26 eV and as well as at 284.02 eV, 284.92 eV, 286.12 eV and 287.42 eV for the 50 % and 90 % samples, respectively [38, 39].
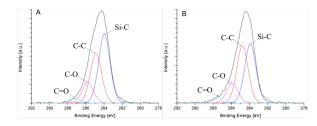
Fig. 15. Deconvolution of C(1s) XPS core level spectrum for films made at 50 % (A) and 90 % (B) of NH$_3$.

The XPS results presented above gave rise to a determination of elemental composition of the coatings shown in Table 2. Simultaneously, calculations have been carried out for the Si(2p) signals in order to establish molecular ratio of Si–N to Si–C structural components of the films. In the case of the 50 % sample, this ratio amounts to approximately 1.4, whereas it rises to 1.6 for the film deposited at 90 % of ammonia in the starting atmosphere. This indicates an increase of silicon-nitrogen bond density, thus constituting a shift towards the optimum Si$_3$N$_4$ structure.

The results obtained indicate that the optimum composition of a gaseous precursor mixture is the one containing 90 % of ammonia. This particular composition results in a maximum of silicon-nitrogen bonding in a film with an accompanying minimum of carbon content. Simultaneously, an increase in the index of refraction and a slight decrease of extinction coefficient are also observed for these coatings. One can, therefore, reason that a maximum of Si$_3$N$_4$ type of material structure is formed under these conditions, thus maximizing the magnitude of refractive index.

3.2.4. Mechanical properties

Results of nanoindentation measurements of a series of Si$_x$N$_y$C$_z$ films, obtained at different concentrations of ammonia in the starting atmosphere, allowed us to draw dependencies of Young modulus and microhardness of these materials on the atomic ratio of nitrogen to silicon in their structure. These dependencies are presented in Fig. 16. It is assumed that theoretical values for pure silicon carbide amount to H = 26 GPa and E = 480 GPa,

while those of pure silicon and carbon nitrides are equal to 33 GPa and 200 GPa and 60 GPa and 250 GPa, respectively [41]. The above values are characteristic of crystalline materials, while the data typical of amorphous coatings are substantially lower [42], more resembling those reported in the present work.
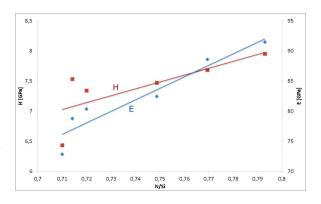

Fig. 16. Dependencies of Young modulus E and microhardness H of Si$_x$N$_y$C$_z$ films on the atomic ratio of nitrogen to silicon.

As seen in the figure, an increase of N/Si ratio in the structure of the coatings is generally followed by a rise of their modulus of elasticity and their hardness. Certain lowering of hardness for films of N/Si ratio around 0.72 may be associated with the effect of hydrogen and a formation of Si–NH–Si bonds. The results acquired are close to the literature data collected for amorphous coatings [42]. In addition, the magnitudes of elasticity index H/E stay in the range of 0.08 to 0.095, often cited in the literature [43–47]. It is close to the theoretical value of 0.1, recognized as a superior one in case of thin solid films.

A nominal critical force, which can be used as a measure of adhesion has been determined with the help of a scratch tests. The results are presented in Table 3.

As seen in Table 3, the critical load stabilizes in the range of 22 mN to 24 mN, and it is larger than that of similar coatings reported in [41]. Independent of the fact that such comparisons should be treated with certain restraint, one should clearly state that the results of mechanical tests of the coatings presented are entirely satisfying in terms

Table 2. Elemental composition of the coatings.

NH$_3$[%]	Atomic composition [%]			
	O	N	C	Si
50	2.72±0.08	23.75±0.67	40.65±0.61	33.45±0.17
60	2.29±0.01	24.24±0.10	39.54±0.33	33.94±0.43
70	2.12±0.06	25.48±0.31	38.36±0.48	34.03±0.08
80	3.39±0.12	24.22±0.88	38.75±0.83	33.64±0.06
90	5.19±0.12	26.05±0.47	35.91±0.82	32.85±0.23
100	4.02±0.05	24.74±0.22	39.10±0.38	32.15±0.11

Table 3. Critical load values recorded for the investigated films.

NH$_3$ [%]	Critical load [mN]
50	27.71±2.09
60	26.98±0.23
70	20.38±1.34
80	23.43±3.59
90	23.69±0.99
100	22.13±2.47

of an application of these coatings in the manufacture of optical filters.

4. Conclusions

The results presented above allow one to conclude that all the coatings obtained in this work exhibit a homogeneous structure along the entire sample and are characterized by satisfying adhesion, with their critical load remaining in the range of 20 mN to 28 mN. Their modulus of elasticity and hardness linearly increase with the increasing nitrogen-to-silicon elemental ratio in the structure.

As the XPS results point to, in the case of the films deposited at and above 50 % of ammonia in the working mixture, the differences in silicon nitrogen and carbon content are rather small. This finding corresponds well to the fact that the refractive index of these materials is nearly constant at the 1.87 to 1.89 level. In addition, it appears that an increased presence of hydrogen bondings, revealed by the FT-IR results obtained for the films deposited in this range of operational conditions, do not have any significant effect on their optical properties.

From the point of view of optical filter production, however, the best properties of the coatings were obtained by applying a precursor atmosphere containing 90 % of ammonia. The refractive index of these films showed the highest value of 1.8871, while their extinction coefficient was equal 5.05×10^{-3}, being one of the top results as well. At the same time, the coatings synthesized under these conditions were characterized with a maximum of nitrogen content in their structure, and a minimum of carbon content. This suggests that the highest molecular fraction of Si$_3$N$_4$ was obtained in this case and that this was a principle effect responsible for the optical properties of the films. Therefore, at the subsequent stage of the project, the RF PECVD conditions selected in the course of the present work will be applied in order to synthesize high refractive index components of rugate interference optical filters.

References

[1] ZAKHVALINSKII V.S., PILIUK E.A., GONCHAROV I. YU., SIMASHKEVICH A.V., SHERBAN D.A., BRUC L.I., CURMEI N.N., RUSU M.I., RODRIGEZ G.V., *Result. Phys.*, 6 (2016), 39.
[2] FENG L., LIU Z., LI Q., SONG W., *Appl. Surf. Sci.*, 252 (2006), 4064.
[3] ZHANG Q., LI X., SHEN J., WU G., WANG J., CHEN L., *Mater. Lett.*, 45 (2000), 311.
[4] CHENG F., M. KELLY S., CLARK S., BRADLEY J.S., BAUMBACH M., SCHÜTZE A., *J. Membr. Sci.*, 280 (2006), 530.

[5] SAYGIN HINCZEWSKI D., HINCZEWSKI M., TEPE-HAN F.Z., TEPEHAN G.G., *Sol. Energ. Mat. Sol. C.*, 87 (2005), 181.

[6] MASSE J.-P., SZYMANOWSKI H., ZABEIDA O., AMASSIAN A., KLEMBERG-SAPIEHA J. E., MARTINU L., *Thin Solid Films*, 515 (2006), 1674.

[7] SZYMANOWSKI H., ZABEIDA O., KLEMBERG-SAPIEHA J.E., MARTINU L., *J. Vac. Sci. Technol. A*, 23 (2005), 241.

[8] LAROUCHE S., SZYMANOWSKI H., KLEMBERG-SAPIEHA J.E., MARTINU L., *J. Vac. Sci. Technol. A*, 22 (2004), 1200.

[9] KOWALSKI J., SZYMANOWSKI H., SOBCZYK-GUZENDA A., GAZICKI-LIPMAN M., *B. Pol. Acad. Sci.-Tech.*, 57 (2009), 171.

[10] ZHANG K., WANG L.S., YUE G.H., CHEN Y.Z, PENG D.L., QI Z.B., WANG Z.C., *Surf. Coat. Tech.*, 205 (2011), 3588.

[11] CHEN C.H., YANG M.R., WU S.K., *Surf. Coat. Tech.*, 202 (2008), 2709.

[12] SCHWARZ F., HAMMER C., THORWARTH G., KUHN M., STRITZKER B., *Plasm. Process. Polym.*, 4 (2007), S254.

[13] VLČEK J., KORMUNDA M., ČÍŽEK J., SOUKUP Z., PEŘINA V., ZEMEK J., *Diam. Relat. Mater.*, 12 (2003), 1287.

[14] CHANG H.L., KUO C.T., *Mater. Chem. Phys.*, 72 (2001), 236.

[15] CHOU T.H., FANG Y.K., CHIANG Y.T., LIN C.I., YANG C.Y., *Sensor. Actuat. A-Phys.*, 147 (2008), 60.

[16] LIMMANEE A., OTSUBO M., SUGIURA T., SATO T., MIYAJIMA S., YAMADA A., KONAGAI M., *Thin Solid Films*, 516 (2008), 652.

[17] KRAUS F., CRUZ S., MÜLLER J., *Sensor. Actuat. B-Chem.*, 88 (2003), 300.

[18] JIMÉNEZ-PÉREZ J.L., ALGATTI M.A., CRUZ SAN MARTIN V., MOREIRA JÚNIOR P.W.P., MOTA R.R.P., CORREA PACHECO Z.N., CRUZ-OREA A., SÁNCHEZ RAMÍREZ J.F., *Mat. Sci. Semicon. Proc.*, 37 (2015), 223.

[19] LU H., CHENG J., *J. Am. Chem. Soc.*, 129 (2007), 14114.

[20] KOLIPAKA K.L., BRUESER V., SCHLUETER R., QUADE A., SCHAEFER J., WULFF H., STRUNSKUS T., FAUPEL F., *Surf. Coat. Tech.*, 207 (2012), 565.

[21] MANOUCHEHRI I., GHOLAMI K., ASTINCHAP B., MORDIAN R., MEHRPARVAR D., *Optik*, 127 (2016), 5383.

[22] KULIKOVSKY V., CTVRTLIK R., VORLICEK V., ZELEZNY V., BOHAC P., JASTRABIK L., *Surf. Coat. Tech.*, 240 (2014), 76.

[23] HOCHE H., PUSCH C., RIEDEL R., FASEL C., KLEIN A., *Surf. Coat. Tech.*, 205 (2010), S21.

[24] CHAKRABORTY M., BANERJEE A., DAS D., *Physica E*, 61 (2014), 95.

[25] JUN K., SHIMOGAKI Y., *Sci. Technol. Adv. Mat.*, 5 (2004), 549.

[26] THEIRICH D., SOLL CH., LEU F., ENGEMANN J., *Vacuum*, 71 (2003), 349.

[27] TOMAR V.K., GAUTAM D.K., *Mat. Sci. Semicon. Proc.*, 10 (2007), 200.

[28] WRÓBEL A.M., KRYSZEWSKI M., GAZICKI M., *Polymer*, 17 (1976), 673.

[29] WRÓBEL A.M., KRYSZEWSKI M., GAZICKI M., *Polymer*, 17 (1976), 678.

[30] GRAY R.C., CARVER J.C., HERCULES D.M., *J. Electron. Spectrosc.*, 8 (1976), 343.

[31] NAYAR P. S., *J. Vac. Sci. Technol. A* 20, 2137 (2002), 2137.

[32] H´ALA M., VERNHES R., ZABEIDA O., KLEMBERG-SAPIEHA J.E., MARTINU L., *J. Appl. Phys.*, 116 (2014), 213302-1.

[33] ANDERSON D.R., *Analysis Silicones*, in: A. LEE SMITH (Ed.), Wiley-Interscience, New York, 1974.

[34] SILVERSTEIN R.M., BASSLER G.C., MORRILL T.C., *Spectrometric identification of organic compounds* (5th Ed.), Wiley, New York, 1991.

[35] LUCOVSKY G., NEMANIH R.J., KNIGHTS J.C., *Phys. Rev. B*, 19 (1979), 2064.

[36] TÉNÉGAL F., GHEORGHIU A., DE LA ROCQUE A., DUFOUR G., SÉNÉMAUND C., DOUCEY B., BAHLOUL-HOURLIER D., GOURSAT P., MAYNE M., CAUCHETIER M., *J. Electron. Spectrosc.*, 109 (2000), 241.

[37] TAYLOR J.A., *Appl. Surf. Sci.*, 7 (1981), 168.

[38] CHEN L.C., BHUSARI D.M., YANG C.Y., CHEN K.H., CHUNG T.J., LIN M.C., CHEN C.K., HUANG Y.F., *Thin Solid Films*, 303 (1997), 66.

[39] SMIRNOVA T.P., BADALIAN A.M., YAKOVKINA L.V., KAICHEV V.V., BUKHTIYAROV V.I., SHMAKOV A.N., ASANOV I.P., RACHLIN V.I., FOMINA A.N., *Thin Solid Films*, 429 (2003), 144.

[40] GÓMEZ F.J., PRIETO P., ELIZALDE E., PIQUERAS J., *Appl. Phys. Lett.*, 69 (1996), 773.

[41] JĘDRZEJOWSKI P., CIŻEK J., AMASSIAN A., KLEMBERG-SAPIEHA J.E., VLCEK J., MARTINU L., *Thin Solid Films*, 447 – 448 (2004), 201.

[42] FERNÁNDEZ-RAMOS C., SÁNCHEZ-LÓPEZ J.C., BELIN M., DONNET C., PASCARETTI F., FERNÁNDEZ A., *Vacuum*, 67 (2002), 551.

[43] DONG-HAU K., DONG-GI Y., *Thin Solid Films*, 374 (2000), 92.

[44] BIELIŃSKI D., WRÓBEL A.M., WALKIEWICZ-PIETRZYKOWSKA A., *Tribol. Lett.*, 13 (2002), 71.

[45] BENDEDDOUCHE A., BERJOAN R., BÊCHE E., HILLEL R., *Surf. Coat. Tech.*, 111 (1999), 184.

[46] CHEN L.C., CHEN K.H., WEI S.L., KICHAMBARE P.D., WU J.J., LU T.R., KUO C.T., *Thin Solid Films*, 355 – 356 (1999), 112.

[47] THÄRIGEN T., LIPPOLD G., RIEDE V., LORENZ M., KOIVUSAARI K.J., LORENZ D., MOSCH S., GRAU P., HESSE R., STREUBEL P., SZARGAN R., *Thin Solid Films*, 348 (1999), 103.

[48] BOVARD B.G., *Appl. Opt.*, 32 (1993), 5427.

[49] WEBSTER F.X., SILVERSTEIN M.R., KIEMLE J.D.,
     BRYCE D.E, *Spectrometric Identification of Organic
     Compounds*, 8th Ed., Wiley, New York, 2015.